



## Article

# Chlorobenzene Mineralization Using Plasma/Photocatalysis Hybrid Reactor: Exploiting the Synergistic Effect

N'Zanon Aly Koné<sup>1,2</sup>, Nacer Belkessa<sup>2</sup>, Youcef Serhane<sup>2</sup>, Sandotin Lassina Coulibaly<sup>1</sup>, Mahamadou Kamagate<sup>1</sup>, Lotfi Mouni<sup>3</sup>, Sivachandiran Loganathan<sup>4,5</sup>, Lacina Coulibaly<sup>1</sup>, Abdelkrim Bouzaza<sup>2</sup>, Abdeltif Amrane<sup>2,\*</sup> and Aymen Amine Assadi<sup>2,6</sup>

- <sup>1</sup> UFR d'Ingenierie Agronomique Forestiere et Environnementale, Université de Man, Man M139PL, Côte d'Ivoire
- <sup>2</sup> École Nationale Supérieure de Chimie de Rennes, CNRS, ISCR (Institut des Sciences Chimiques de Rennes)–UMR 6226, Université Rennes, F-35000 Rennes, France
- <sup>3</sup> Laboratoire de Gestion et Valorisation des Ressources Naturelles et Assurance Qualité, Université Akli Mohand Oulhadj, Bouira 10000, Algeria
- <sup>4</sup> Laboratory of Plasma Chemistry and Physics (LPCP), Department of Chemistry, Faculty of Engineering and Technology, SRM Institute of Science and Technology, SRM Nagar, Kattankulathur, Chennai 603203, India
- <sup>5</sup> Plasma Research Laboratory, Center for Air and Aquatic Resources Engineering & Science, Department of Chemical and Biomolecular Engineering, Clarkson University, Potsdam, NY 13699, USA
- <sup>6</sup> College of Engineering, Imam Mohammad Ibn Saud Islamic University, IMSIU, Riyadh 11432, Saudi Arabia
- \* Correspondence: abdelatif.amrane@univ-rennes1.fr

**Abstract:** Mineralization of gaseous chlorobenzene (major VOC from cement plants) was studied in a continuous reactor using three advanced oxidation processes: (i) photocatalysis, (ii) Dielectric Barrier Discharge (DBD) plasma and (iii) DBD/TiO<sub>2</sub>-UV coupling. The work showed an overproduction of OH<sup>\*</sup> and O<sup>\*</sup> radicals in the reaction medium due to the interaction of Cl<sup>\*</sup> and O<sub>3</sub>. A parametric study was carried out in order to determine the evolution of the removal efficiency as a function of the concentration, the flow rate and the applied voltage. Indeed, a variation of the flow rate from 0.25 to 1 m<sup>3</sup>/h resulted in a decrease in the degradation rate from 18 to 9%. Similarly, an increase in concentration from 13 to 100 mg/m<sup>3</sup> resulted in a change in degradation rate from 18 to 4%. When the voltage was doubled from 6 to 12 kV, the degradation rate varied from 22 to 29 % (plasma) and from 53 to 75% (coupling) at 13 mg/m<sup>3</sup>. The evolution of CO<sub>x</sub> and O<sub>3</sub> was monitored during the experiments. When the voltage was doubled, the selectivity increased from 28 to 37% in the plasma alone and from 48 to 62 % in the coupled process. In addition, at this same voltage range, the amount of ozone formed varied from 10 to 66 ppm in plasma and 3 to 29 ppm in coupling. This degradation performance can be linked to a synergistic effect, which resulted in an increase in the intensity of the electric field of plasma by the TiO<sub>2</sub> and the improvement in the performance of the catalyst following the bombardment of various high-energy particles of the plasma.

**Keywords:** synergistic effect; air cement plants; plasma; photocatalysis; reactive species



**Citation:** Koné, N.A.; Belkessa, N.; Serhane, Y.; Coulibaly, S.L.; Kamagate, M.; Mouni, L.; Loganathan, S.; Coulibaly, L.; Bouzaza, A.; Amrane, A.; et al. Chlorobenzene Mineralization Using Plasma/Photocatalysis Hybrid Reactor: Exploiting the Synergistic Effect. *Catalysts* **2023**, *13*, 431. <https://doi.org/10.3390/catal13020431>

Academic Editors: Eduardo Miró, Ezequiel David Banus and Juan Pablo Bortolozzi

Received: 28 January 2023

Revised: 11 February 2023

Accepted: 12 February 2023

Published: 16 February 2023



**Copyright:** © 2023 by the authors. Licensee MDPI, Basel, Switzerland. This article is an open access article distributed under the terms and conditions of the Creative Commons Attribution (CC BY) license (<https://creativecommons.org/licenses/by/4.0/>).

## 1. Introduction

Cement is a finely ground, inorganic, non-metallic powder that is a basic material in the construction industry. The high production of cement results in the release of various Volatile Organic Compounds (VOCs) into the atmosphere [1]. These substances are often highly volatile, even at room temperature, and represent a major risk to the environment. Indeed, these compounds cause numerous environmental consequences such as acidification of the atmosphere, depletion of the ozone layer and increase in the greenhouse effect [2–5]. Emissions of these gaseous pollutants also pose a significant health risk to workers in these industries [6–8]. These compounds are also a source of discomfort for the population as well as potential sources of conflict. They also contaminate

the orchards of plants, which become less productive. The United States Environmental Protection Agency and the European Commission have identified chlorobenzene (CB) as a priority pollutant to monitor [9]. This pollutant is carcinogenic to humans, according to the international agency for research on cancer classification [10]. With the increasing attention to environmental protection, especially air pollution control, industries and research organizations are facing great challenges to develop technologies to effectively remove this compound without generating secondary pollutants. In comparison with other VOCs categories, Cl-VOCs show a lower biodegradability, higher stability and toxicity [9].

To remedy this problem, Advanced Oxidation Processes (AOPs) have been developed. AOPs can eliminate the Cl-VOCs efficiently by generating powerful hydroxyl radicals, which possess strong oxidizability. AOPs are interesting and promising solutions for air pollution treatment and include photocatalysis and cold plasma as widely used technologies [11–14]. Cold plasma is a generally electrically neutral gas mixture containing photons, charged particles (ion or electron) and neutral particles (molecules, atoms and radicals), mostly in excited states [15,16]. Dielectric barrier discharges, which were implemented in this study, are obtained by applying a high potential difference between two electrodes separated by a dielectric. Photocatalysis consists of oxidizing the pollutant on a catalyst (usually  $\text{TiO}_2$ ) under UV radiation [17–19]. In the presence of oxygen and/or water vapor, the UV radiation that activates the semiconductor (catalyst) allows the VOCs in contact with the reactive surface to be transformed into  $\text{CO}_2$  and  $\text{H}_2\text{O}$  [18,20,21]. Cold-plasma-assisted photocatalysis has recently been considered an attractive alternative due to its non-equilibrium nature, low energy cost and unique ability to initiate physical and chemical reactions at low temperatures [22–24]. Therefore, cold-plasma-assisted photocatalysis can be an ideal method for CB decomposition, as the active species can enhance the chemical bond breaking of the pollutant, resulting in higher conversion efficiency. The elimination of VOCs in a cold-assisted catalysis system has been reviewed from different perspectives in the literature [25–27]. However, the increase in VOC degradation rates obtained by studies of the coupling DBD plasma and photocatalysis has led to the implementation of many research projects on this topic [28–31]. Indeed, the introduction of an external UV lamp into the plasma significantly improves the degradation rate. By increasing the applied voltage, the electric field in the reactor can be improved, resulting in a higher degree of ionization of the chemical species. As a result, the pollutant is more likely to be attacked by electrons or radicals [32]. This leads to a higher removal of the VOC [33]. These high removal rates are also due to the influence of the catalysts on the physico-chemical properties of the plasma discharge and that of the plasma discharge on the performance of the catalyst. It is with this in mind that the present study was carried out. This work consisted of treating a chlorinated aromatic VOC in a cylindrical reactor by photocatalysis and plasma. The main objectives of this work were (i) to study the degradation of chlorobenzene (CB) by photocatalysis ( $\text{TiO}_2$ ), DBD plasma and coupling DBD/ $\text{TiO}_2$ -UV; (ii) to evaluate the quantities of  $\text{CO}_x$  and  $\text{O}_3$  produced. The work was carried out on a continuous reactor, allowing us to directly carry out the analysis during the degradation.

## 2. Results and Discussion

### 2.1. Photocatalytic Removal of CB

Figure 1 shows the CB removal efficiency (RE) and degradation rate (DR) for various initial concentrations. The experiments were carried out at a constant flow rate of  $0.25 \text{ m}^3/\text{h}$  and with 5% RH. It was observed that CB was significantly removed by the photocatalytic process. The RE decreased from 18 to 4% when the CB concentration was increased from 13 to  $100 \text{ mg}/\text{m}^3$ . These results showed that the degradation efficiency decreased with increasing initial CB concentrations. This trend could be explained by the increase in the ratio of active sites to the amount of CB molecules; the high amount of CB molecules reduces the number of active sites available on the catalyst surface and quickly consumes the produced reactive species [29,34]. Similar results were observed by [35] while treating indoor air using a luminous photocatalytic textile. The authors of [19] found the same

result during gaseous ethylbenzene removal by photocatalytic  $\text{TiO}_2$ . They concluded that the increase in ethylbenzene inlet concentration leads to a significant diminution of the removal efficiency.

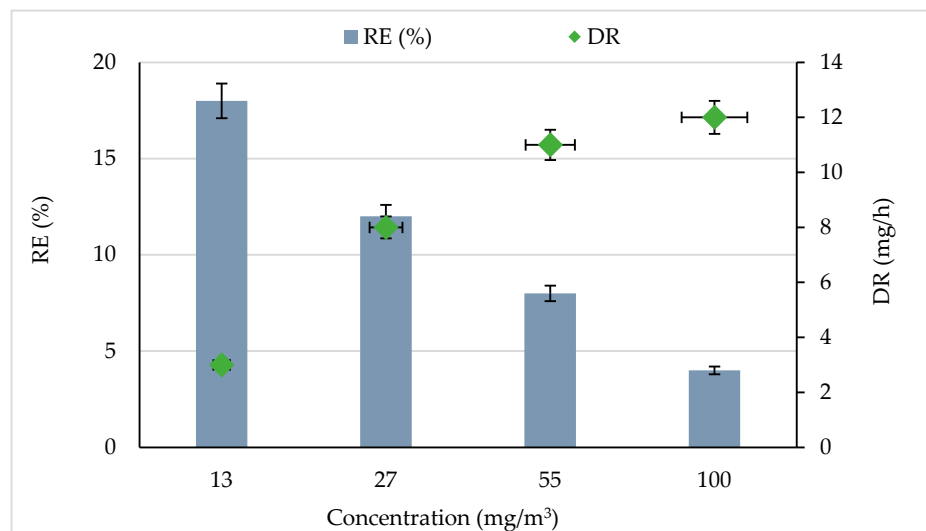
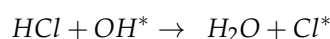
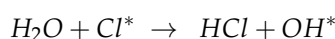
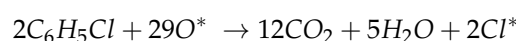
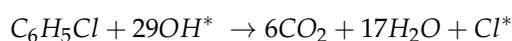
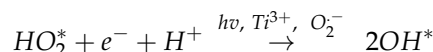
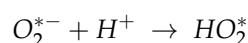
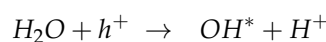
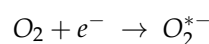
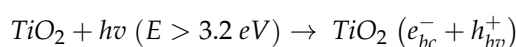


**Figure 1.** Effect of CB concentration on removal efficiency and degradation rate. Experimental conditions were RH = 5%, Temperature = 20 °C, and total flow rate = 0.25 m<sup>3</sup>/h.

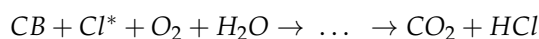
An increase in CB concentration significantly improved the degradation rate (Figure 1). The degradation rate increased from 3 to 12 mg/h with increasing the CB concentration from 13 to 100 mg/m<sup>3</sup>. This result could be attributed to the high mass transfer into the reactor per unit of time; hence degradation enhanced [36,37]. Under UV radiation CB was degraded by the heterogeneous photocatalytic process according to the following equations [18,38,39]. The authors of [40] showed the variation of the RE of butyraldehyde by photocatalysis as a function of the input concentration. They noted that the RE of butyraldehyde increased when the concentration of pollutant was increased. Since the photocatalysis reaction is often equated to a pseudo-first-order reaction, this means that a higher flow of pollutants (due to an increase in the inlet concentration) naturally induces an increase in the degradation kinetics [41]. Of course, for a constant amount of catalyst, the percentage of degradation and mineralization decreases when these operating parameters increase.



The HO\* radicals are highly reactive electrophilic species, which could attack the 2, 3 and 4 positions on the aromatic ring. OH\* is an electron-donating group. The positive hole attacks this position to cleave the aromatic ring. This reaction mechanism has been detailed

by [42]. The first  $Cl^*$  species present on the catalyst generate degradation sequences by attacking the adsorbed CB. Moreover,  $OH^*$  radicals could also react with  $Cl^*$  radicals and produce  $O_2^{-*}$ , which is a powerful oxidant to mineralize the CB on the  $TiO_2$  surface [43,44].

Many studies have shown that photocatalytic degradation of chlorinated VOCs can take place by both  $OH^*$  and  $Cl^*$  radicals. A comparison of kinetic data for  $VOC + OH^*$  reaction and  $VOC + Cl^*$  reaction suggests that the latter reaction is faster [45].



When the amount of  $O_2$  is limited in the reaction media, the valence band electron attacks the C-Cl bond. In this case, dechlorination takes place before the aromatic ring is broken. The  $Cl^*$  radicals can then initiate a series of radical chain reactions and compensate for the negative effect caused by the high CB concentration.

## 2.2. Effect of Feed Flow Rate on CB Degradation Rate

Under constant CB concentration ( $13 \text{ mg/m}^3$ ) and RH (5%), the feed flow rate varied between  $0.25$  and  $1 \text{ m}^3/\text{h}$ , and the corresponding RE and DR are reported in Figure 2. The increase in feed flow rate showed a negative effect on the removal efficiency since the RE decreased from 18 to 9% when the flow rate increased from  $0.25$  to  $1 \text{ m}^3/\text{h}$ . The decrease in RE can be correlated to the CB residence time in the reactor, which decreased from 10.05 to 2.51 s. The small residence time considerably reduces the contact time between pollutants and  $HO^*$  and  $O^*$  radicals on the  $TiO_2$  surface. Thus, the amount of pollutants capable of reacting with the active species attached to the catalyst surface is reduced [46,47]. In addition, the amount of  $HO^*$  and  $O^*$  radicals produced on the  $TiO_2$  surface also decreases by limiting the following reactions (i)  $O_2$  and electrons, and (ii)  $H_2O$  and  $h^+$  on the  $TiO_2$  surface [48]. Figure 2 shows an improvement in the degradation rate as the concentration increased. This enhancement is linked to radical species formation, i.e., if the first radical species formation is made easier, the degradation of adsorbed pollutants starts quicker and the residence time could be shorter [45].

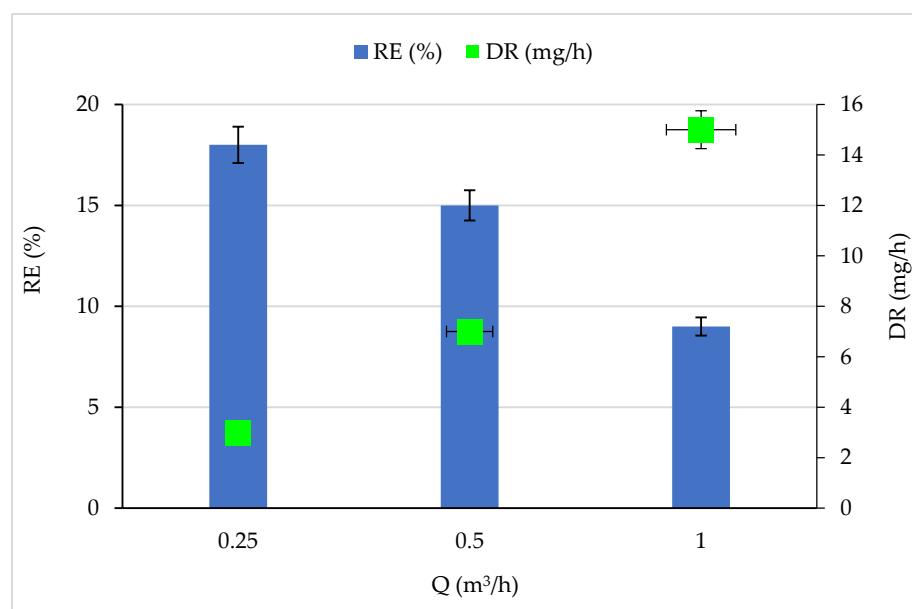


**Figure 2.** Effect of feed flow rate on CB removal efficiency and degradation rate. Experimental conditions: RH: 5%, T:  $20 \text{ }^\circ\text{C}$  and C:  $13 \text{ mg/m}^3$ .

The same results were found by [41] when treating volatile organic compounds by photocatalytic oxidation. The authors of [49] studied the degradation of oxalic acid in a photocatalytic reactor. They conclude that the degradation efficiency of oxalic acid in the

photocatalytic reactor decreased with the increase in flow rates, changing from 50% to 40% when the flow rate was varied from  $2.5 \text{ m}^3 \cdot \text{h}^{-1}$  to  $10 \text{ m}^3 \cdot \text{h}^{-1}$ .

### 2.3. Exploiting the Synergistic Effect: Photocatalysis and Plasma-Photocatalysis Combined Processes

The effect of plasma discharge (in the absence of UV light) and combined process (photocatalysis + plasma discharge) on CB removal efficiency (RE) were studied for various CB concentrations and reported in Figure 3. The plasma input voltage varied between 6 and 12 kV, and the CB concentration was also changed from  $13 \text{ mg/m}^3$  to  $27 \text{ mg/m}^3$ . It was observed that the combined process showed higher CB conversion as compared to individual photocatalysis and plasma process for all studied CB feed concentrations and plasma applied voltage. For example, with  $13 \text{ mg/m}^3$  inlet concentration and 12 kV, 75% removal efficiency was obtained, which was about 57% more than photocatalysis (18%) and 55% more than the plasma process (20%). This finding emphasizes that a synergistic effect was observed between photocatalysis and the plasma-photocatalysis process.

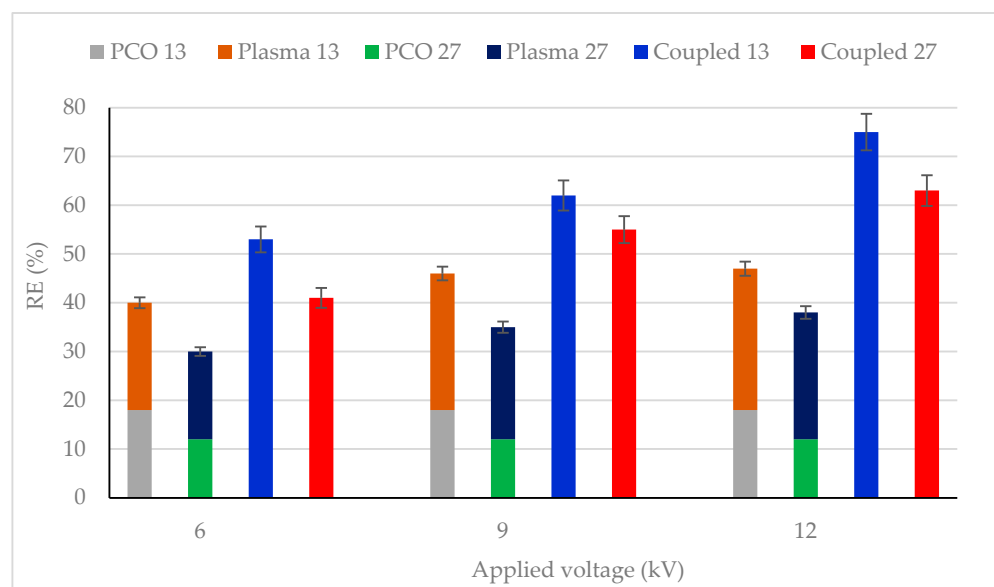


**Figure 3.** CB removal efficiency for photocatalysis, plasma-catalysis and photocatalysis-plasma-catalysis combined process. CB inlet concentration: 13 and  $27 \text{ mg/m}^3$ , Flow rate:  $0.25 \text{ m}^3/\text{h}$ , RH: 5%, Temperature:  $20 \text{ }^\circ\text{C}$ , Plasma applied frequency: 50 Hz.

An increase in plasma applied voltage increased the RE for all CB feed flow concentrations. This phenomenon can be attributed to the formation of more oxidative species ( $\text{OH}^*$  and  $\text{O}^*$ ) on the  $\text{TiO}_2$  surface, leading to enhanced removal [48,50]. Similar results have also been reported by [51–53].

The synergistic effect observed between photocatalysis and plasma discharge is closely related to the influence of the catalysts on plasma discharge characteristics and the effect of plasma discharge on the physico-chemical properties of the catalysts. It can be suggested that the packed catalyst in the discharge zone would affect the plasma discharge by the following mechanisms.

The catalysts could considerably increase the electric field strength. When  $\text{TiO}_2$  particles are in contact with an electrode, the micro-discharges could be formed on the catalyst surface and inside the pores in the discharge region. Thus, the local electric field strength and electrode temperature could significantly increase in the discharge zone [27–29].

The active species formed during the single plasma discharge do not play an important role in CB conversion due to their short existence time and low energy ( $<2 \text{ eV}$ ). CB molecules are not effectively destroyed by these species because of their high binding energies.

However, increasing the electric field strength allows the active species to reach the energy level needed to break the bonds between CB molecules [23,30].

Plasma discharges also improve the performance of catalysts. Since the temperature of electrons is >104 K, the physical and chemical properties of the catalysts are likely to be altered due to the bombardment of various high-energy particles on the catalyst. The surface or internal structure of the catalyst changes. Indeed, the sizes of catalytically active particles decrease, and the distribution of particles becomes uniform over the catalyst surface. These variations increase the active surfaces and improve the stability of the catalyst [54,55].

Under these reaction conditions, in addition to the radicals produced by plasma and classical photocatalysis, successive photocatalytic reactions take place on the TiO<sub>2</sub> surface. These reactions increase the production of HO<sup>\*</sup> and O<sup>\*</sup> radical species from plasma-produced O<sub>3</sub>, thus increasing the conversion rate of CB molecules. The work of [56] also corroborates this finding.

Ref. [57] Investigated the synergistic effect of toluene degradation in surface dielectric barrier discharge/photocatalytic reactor with mesh electrode. The results showed that TiO<sub>2</sub> and UV irradiation both presented promoting effect on toluene degradation in photocatalysis/DBD reactor with mesh electrodes. The degradation efficiency of toluene was also enhanced with the introduction of TiO<sub>2</sub> and UV irradiation. Increases in toluene degradation efficiency of 26.8% was obtained at SIE of 300 J·L<sup>-1</sup>. When both TiO<sub>2</sub> and UV were applied, the enhancement could rise to 41.6%.

Ref. [58] used a uniform and stable dielectric barrier discharge plasma for the degradation of benzene combined with a transition metal oxide catalyst. The effects of catalyst types, applied voltage, driving frequency and initial VOCs concentration on the degradation efficiency of benzene were studied. It was found that the addition of packed dielectric materials can effectively improve the uniformity of discharge and enhance the intensity of discharge, thus promoting the benzene degradation efficiency. At 22 kV, the degradation efficiencies of dielectric barrier discharge plasma packed with CuO, ZnO and Fe<sub>3</sub>O<sub>4</sub> were 93.6%, 93.2% and 76.2%, respectively. When packing with ZnO, the degradation efficiency of the dielectric barrier discharge plasma was improved from 86.8% to 94.9% as the applied voltage increased from 16 kV to 24 kV. The synergistic mechanism and the property of the catalyst were responsible for benzene degradation in the plasma-catalysis system.

Ref. [59] proposed a hybrid system that combined dielectric barrier discharge plasma with catalysis (DPC) for toluene degradation. To improve the performance of DPC, photocatalysts TiO<sub>2</sub> were doped by Mn and Fe, respectively. The best doping ratios of Mn and Fe were both 1.0%. The increase in electric field intensity in the range of 6.9–10.3 kV/cm could favor the synergism for DPC significantly, but the ascending AC frequency failed to achieve that. Mn-DPC and Fe-DPC both could maintain the high toluene degradation efficiency when gas flow rate and initial concentration increased from 2.5 to 10.1 cm/s and from 700 to 2300 mg/cm<sup>3</sup>, respectively. Fe-DPC showed slightly better performances than Mn-DPC in degradation efficiency.

#### 2.4. CB Mineralization: Photocatalysis, Plasma Catalysis and Combined Process

CO<sub>x</sub> selectivity was determined for all the processes using the following equation.

$$CO_x \text{ selectivity} = \frac{[CO_x]_{in} - [CO_x]_{out}}{N_c \times RE (\%) \times [CB]_{in}} \times 10^4 \quad (1)$$

$N_c = 6$  (the number of carbon atoms in chlorobenzene),  $RE (\%)$  removal efficiency,  $x = 1$  for CO and  $x = 2$  for CO<sub>2</sub>,  $[CO_x]_{in}$  and  $[CO_x]_{out}$  are the CO<sub>x</sub> concentrations at the inlet and outlet of the reactor in ppm.  $[CB]_{in}$  is the CB concentration at the inlet in ppm.

Interestingly, continuous analysis at the reactor outlet revealed that CO was not quantified either in photocatalytic or in a combined process. The CO concentrations were measured with a NO/CO ZRE gas analyzer.



Figure 4 reports the CO<sub>2</sub> selectivity for photocatalysis, plasma and combined process for various plasma applied voltage. About 70% of CO<sub>2</sub> selectivity was reached for the photocatalysis process. The missing carbon mass balance can be attributed to the partially oxidized species produced by the photocatalytic process, which were not quantified by GC. However, the CO<sub>2</sub> selectivity could be increased by increasing the UV power density and decreasing the feed flow rate.

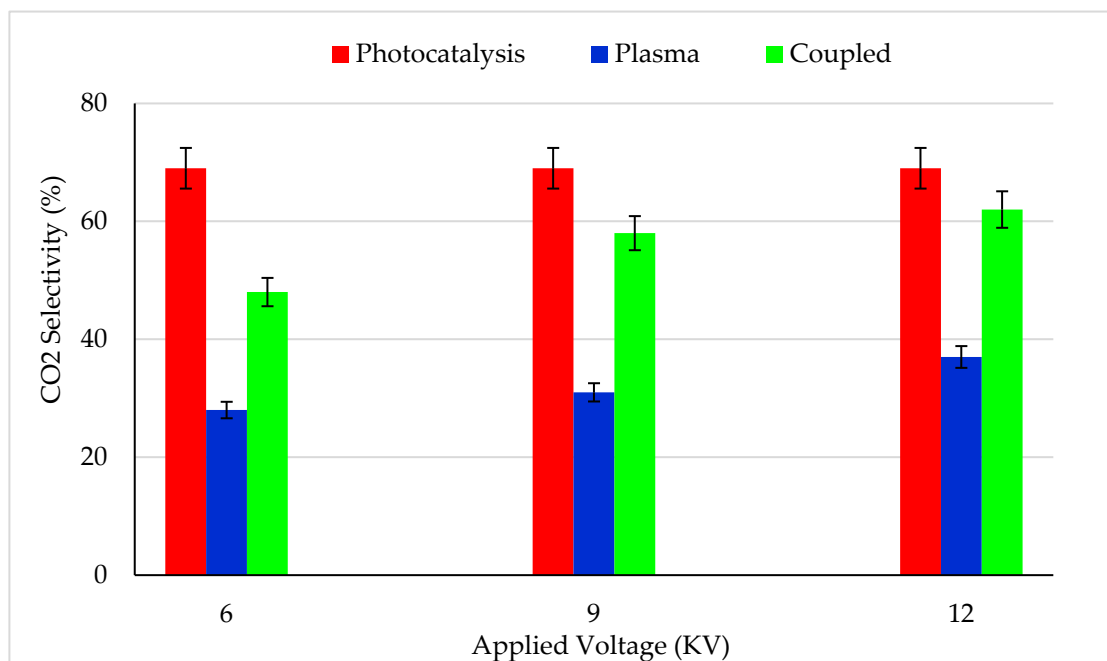


**Figure 4.** CO<sub>2</sub> selectivity for (i) photocatalysis, (ii) plasma-catalysis and (iii) Photocatalysis-plasma-catalysis combined process. CB inlet concentration: 13 mg/m<sup>3</sup>, Flow rate: 0.25 m<sup>3</sup>/h, RH: 5%, Temperature: 20 °C, Plasma applied frequency: 50 Hz.

With a 6 kV input voltage, only 28% CO<sub>2</sub> selectivity was reached (Figure 4), which was 2.5 times lower than the CO<sub>2</sub> selectivity reached by the photocatalysis process. An increase in plasma applied voltage from 6 to 12 kV increased the CO<sub>2</sub> selectivity from 28 to 37% [31,54,60]. Even though the plasma alone process exhibited higher CB removal efficiency (Figure 3) than photocatalysis, the mineralization efficiency was very low. It implies the fact that plasma applied voltage was not sufficient to achieve complete mineralization.

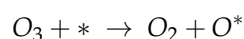
Interestingly, when plasma (12 kV) was coupled with photocatalysis, 62% CO<sub>2</sub> selectivity was reached, which was 7% lower than achieved by the photocatalysis alone process [51,61–63]. It should be mentioned that a synergistic effect was not observed for CO<sub>2</sub> selectivity. High CB removal efficiency and low CO<sub>2</sub> selectivity of the combined process could be explained by the following hypotheses:

- (i) In the photocatalytic process, the CB conversion and mineralization take place on the TiO<sub>2</sub> surface. Thus, most of the adsorbed CB were completely oxidized to CO<sub>2</sub> and eventually desorbed into the gas phase.
- (ii) In the combined process, plasma-assisted CB conversion in the gas phase dominates the photocatalytic removal on the TiO<sub>2</sub> surface. Moreover, the gas phase conversion perhaps leads to the formation of partially oxidized products such as formic acid, acetic acid and other products. These species are not completely mineralized under the given operating conditions and lead to low CO<sub>2</sub> selectivity. Further investigation is needed to confirm these hypotheses and to improve CO<sub>2</sub> selectivity.
- (iii) UV radiation probably decreases the amount of reactive species production under plasma discharge.

### 2.5. Evaluation of Ozone Formation in Plasma and Coupled Process

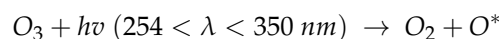
Ozone is a long-lived reactive species produced by plasma discharge in the gas phase. Ozone concentration at the reactor downstream was quantified for plasma and plasma-photocatalytic combined process and reported in Figure 5. Under similar operating conditions plasma alone process produced about 2 folds more ozone (with 12 kV, 66 ppm) than the combined process (plasma + photocatalysis), i.e., 29 ppm. An increase in plasma applied voltage (6 to 12 kV) increased the ozone concentration (10 to 66 ppm) due to a high number of micro discharges in the gas phase. The decrease in ozone production in the combined process could be explained by the following mechanisms.

- (i) On the active sites of  $\text{TiO}_2$  surface [64],  $\text{O}_3$  is decomposed to  $\text{O}_2$  and adsorbed  $\text{O}^*$  radicals [55,65]:



\* : active sites

- (ii) UV radiation also promotes the decomposition of  $\text{O}_3$  through the following reaction. [51]



- (iii) The high presence of  $\text{Cl}^*$  radicals also contributes to  $\text{O}_3$  scavenging according to the following reaction [66].

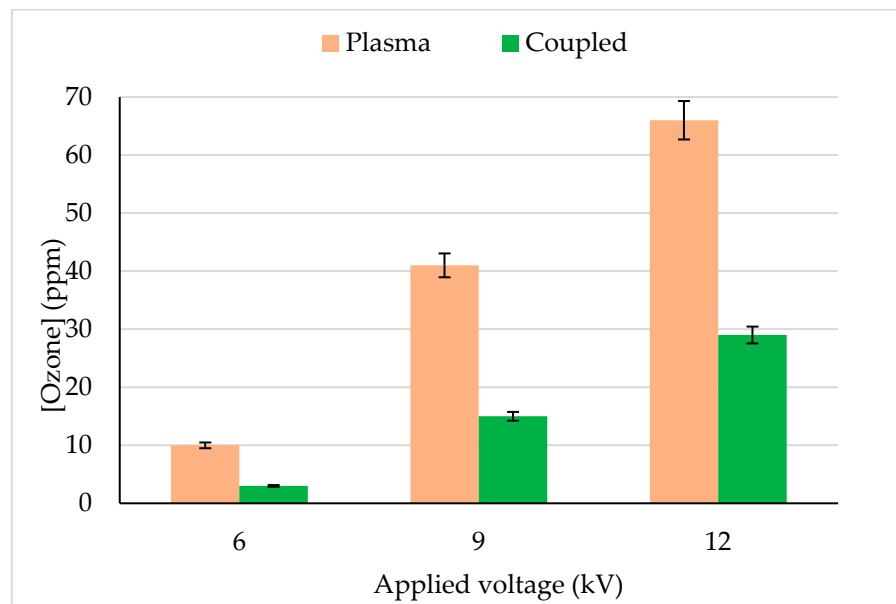
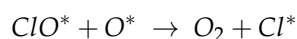
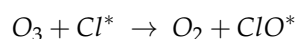


**Figure 5.** Ozone concentration quantified at the reactor outlet during CB degradation in plasma and the coupling process. CB inlet concentration:  $13 \text{ mg/m}^3$ , Flow rate:  $0.25 \text{ m}^3/\text{h}$ , RH: 5%, Temperature:  $20 \text{ }^\circ\text{C}$ , Plasma applied frequency: 50 Hz.

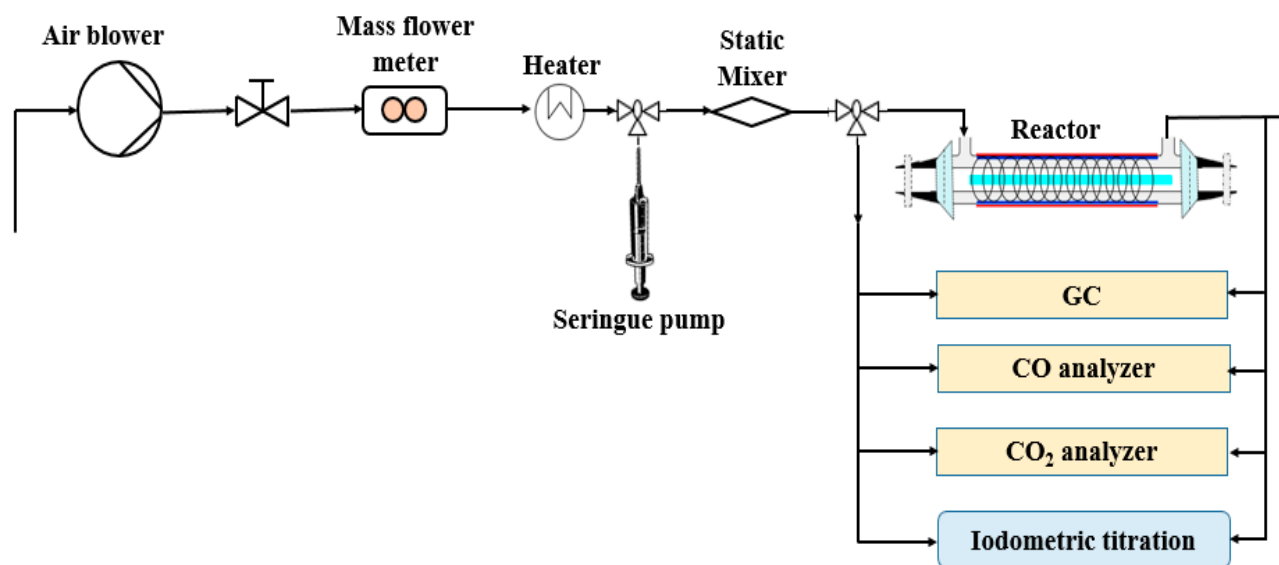
These mechanisms show that ozone significantly contributed to the CB removal during the coupling process. This result is consistent with those obtained by [64].



### 3. Experimental Setup

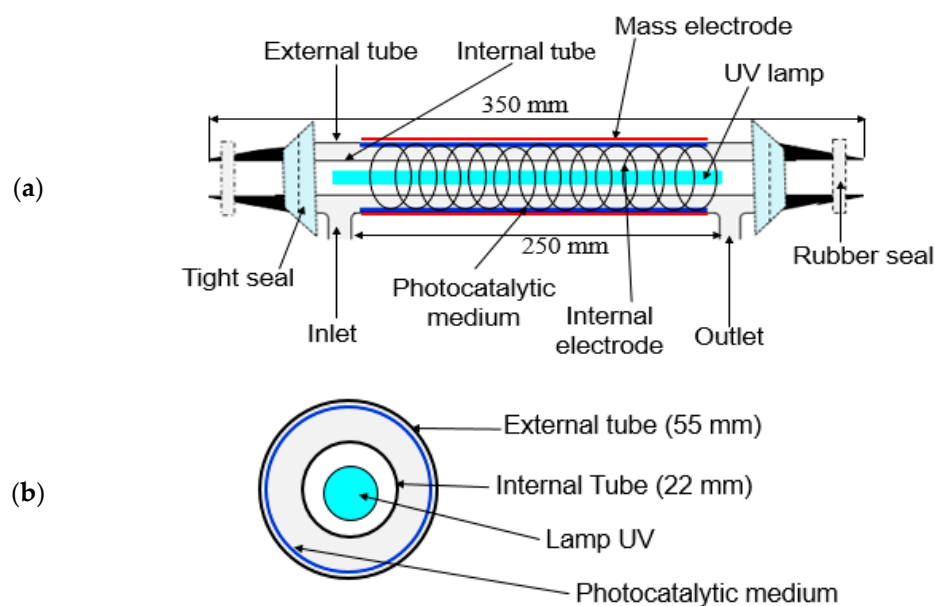
#### 3.1. UV and Plasma Reactor Configuration

Figure 6 shows the general schematic of the experimental setup and analytical devices. The reactor was designed to be used for (i) photocatalysis, (ii) plasma and (iii) the coupling process. The process was equipped with a polluted air generation system, cylindrical reactor, gas sampling equipment and analysis systems. The reactor consisted of two concentric cylindrical Pyrex glass tubes with 350 mm in length and outer diameters of 55 and 22 mm (Figure 7a,b). The gap between the two tubes is packed with TiO<sub>2</sub>-loaded glass fiber fabric (GFT, Ahlstrom Research and Services). The copper plate wrapped outside of the bigger tube was used as a ground electrode. The inner electrode was made from a continuous helical aluminum winding. This electrode was a 2-mm thick helicoid wire electrode shaped like a coil spring in close contact with the inner wall of the reactor (12 turns in 250 mm). The gaseous effluent flowed through the interannular space, which corresponds to the grey area in the figure cited below. The light source used was an 80 W UV lamp (Philips CLEO performance). Its emission spectrum varied from 300 to 400 nm. This configuration is called double dielectric barrier discharge (D-DBD). Plasma discharge was ignited using an AC power source (3 to 6 V, BFi OPTILAS, France). This voltage was amplified between 6 and 12 kV using an external amplifier (TREK\_30 kV model 30/20A, 190 Walnut Street • Lockport, NY 14094 • USA). Plasma-injected power was monitored using the Lissajous method [67].



**Figure 6.** General schematic of the experimental setup.

For the photocatalytic and combined process, the UV lamp was placed in the inner cylinder in order to obtain uniform irradiation on the catalyst surface. A detailed description of polluted air stream generation is reported by [11]. Chlorobenzene (CB) was injected by an infusion syringe pump (3  $\mu\text{L}/\text{h}$ ) to obtain 13  $\text{mg}/\text{m}^3$  concentration in 4.166  $\text{mL}/\text{min}$  total flow rate.



**Figure 7.** (a) Schematic of the reactor setup and (b) cross-section of the concentric cylindrical Pyrex glass tube reactor.

### 3.2. Gas Phase Analysis

The CB concentration, before and after mineralization experiments, was quantified using a gas chromatograph (GC, Thermo Focus, Carlsbad, CA, USA) equipped with a 60 m × 0.25 mm polar DB-MS capillary column (film thickness: 0.25 mm). The GC operating conditions were: flame ionization detector (FID), carrier gas at a flow rate: 1 mL/min<sup>-1</sup>, injector and detector temperature is: 250 °C. Samples were collected at the reactor downstream using a 500 µL gas-tight syringe and manually injected into the GC.

The CO<sub>2</sub> concentration was quantified using a multi-gas infrared analyzer equipped with GFC (Gas Filters Correlation) technology (MIR 9000 Environment SA). O<sub>3</sub> concentration was measured by the iodometric titration method [64]. Temperature and relative humidity (RH) were monitored by a TESTO sensor.

The CB removal efficiency (RE) and degradation rate (DR) are calculated using the following equations.

$$RE = \frac{C_{in} - C_{out}}{C_{in}} \times 100 \quad (2)$$

$$DR = (C_{in} - C_{out}) \times Q \quad (3)$$

where  $C_{in}$  and  $C_{out}$  are the initial and final concentrations of CB, and  $Q$  is the total feed flow rate.

## 4. Conclusions

In this study, the degradation of CB in the gas phase was studied in photocatalysis, plasma and plasma/TiO<sub>2</sub>-UV combined process. The degradation of CB was influenced by the concentration, feed flow rate and the voltage injected into the reactor. Comparatively, the DBD/TiO<sub>2</sub> coupling showed a better removal efficiency ranging from 53 to 75% (13 mg/m<sup>3</sup>) and from 41 to 63% (27 mg/m<sup>3</sup>) when the plasma input voltage was increased from 6 to 12 kV. Under similar operating conditions, synergistic effect was observed for CB removal.

This performance can be related to the changes brought by the catalyst on plasma discharge characteristics and vice versa. In addition, the study revealed that Cl\* radicals are also involved in CB decomposition. It was also shown that OH\* radicals react with Cl\* in the medium to produce O\*, another more powerful oxidant, which could mineralize the adsorbed CB.

**Author Contributions:** N.A.K., N.B. and Y.S.: investigation, formal analysis, visualization and writing—original review. S.L.C., M.K., A.A., L.M. and S.L.: conceptualization, funding acquisition, methodology and resources. L.C., A.B. and A.A.A.: project administration, supervision and writing—review and editing. All authors have read and agreed to the published version of the manuscript.

**Funding:** This research received no external funding.

**Institutional Review Board Statement:** Not applicable.

**Informed Consent Statement:** Not applicable.

**Data Availability Statement:** Not applicable.

**Conflicts of Interest:** The authors declare that they have no conflict of interest.

## References

1. Misra, N.N.; Yepez, X.; Xu, L.; Keener, K. In-package cold plasma technologies. *J. Food Eng.* **2019**, *244*, 21–31. [[CrossRef](#)]
2. Devi, K.S.; Lakshmi, V.V.; Alakanandana, A. Impacts of Cement Industry on Environment—an Overview. *Asia Pac. J. Res. ISSN* **2017**, *1*, 2347–4793.
3. Whalley, L.K.; Slater, E.J.; Woodward-Massey, R.; Ye, C.; Lee, J.D.; Squires, F.; Hopkins, J.R.; Dunmore, R.E.; Shaw, M.; Hamilton, J.F.; et al. Evaluating the sensitivity of radical chemistry and ozone formation to ambient VOCs and NO<sub>x</sub> in Beijing. *Atmos. Chem. Phys.* **2021**, *21*, 2125–2147. [[CrossRef](#)]
4. Choi, M.S.; Qiu, X.; Zhang, J.; Wang, S.; Li, X.; Sun, Y.; Chen, J.; Ying, Q. Study of Secondary Organic Aerosol Formation from Chlorine Radical-Initiated Oxidation of Volatile Organic Compounds in a Polluted Atmosphere Using a 3D Chemical Transport Model. *Environ. Sci. Technol.* **2020**, *54*, 13409–13418. [[CrossRef](#)] [[PubMed](#)]
5. Li, N.; Xing, X.; Cheng, J.; Zhang, Z.; Hao, Z. Influence of oxygen and water content on the formation of polychlorinated organic by-products from catalytic degradation of 1,2-dichlorobenzene over a Pd/ZSM-5 catalyst. *J. Hazard. Mater.* **2021**, *403*, 123952. [[CrossRef](#)] [[PubMed](#)]
6. Wallenius, K.; Hovi, H.; Remes, J.; Mahiout, S.; Liukkonen, T. Volatile Organic Compounds in Finnish Office Environments in 2010–2019 and Their Relevance to Adverse Health Effects. *Int. J. Environ. Res. Public Health* **2022**, *19*, 4411. [[CrossRef](#)] [[PubMed](#)]
7. Marano, F. Les expositions humaines contrôlées aux gaz d'échappement des moteurs diesel: Résultats des effets sur la santé de la pollution atmosphérique et orientations futures. *Environ. Risques Santé* **2022**, *21*, 385–387.
8. Pineau, P.-O.; Gauthier, P.; Whitmore, J.; Normandin, D.; Beaudoin, L.; et Beaulieu, J. *Portrait et pistes de réduction des émissions industrielles de gaz à effet de serre au Québec: Volet 1-Projet de recherche sur le potentiel de l'économie circulaire sur la réduction de gaz à effet de serre des émetteurs industriels québécois*; HEC Montréal: Montreal, QC, Canada, 2019.
9. Mu, Y.; Williams, P.T. Recent advances in the abatement of volatile organic compounds (VOCs) and chlorinated-VOCs by non-thermal plasma technology: A review. *Chemosphere* **2022**, *308*, 136481. [[CrossRef](#)]
10. World Health Organisation. *IARC Monographs on the Identification of Carcinogenic Hazards to Humans*; World Health Organisation: Geneva, Switzerland, 2019.
11. Zhao, J.; Sun, J.; Meng, X.; Li, Z. Recent Advances in Vehicle Exhaust Treatment with Photocatalytic Technology. *Catalysts* **2022**, *12*, 1051. [[CrossRef](#)]
12. Palma, D.; Richard, C.; Minella, M. State of the art and perspectives about non-thermal plasma applications for the removal of PFAS in water. *Chem. Eng. J. Adv.* **2022**, *10*, 100253. [[CrossRef](#)]
13. Ye, Z.; Zhao, L.; Nikiforov, A.; Giraudon, J.-M.; Chen, Y.; Wang, J.; Tu, X. A review of the advances in catalyst modification using nonthermal plasma: Process, Mechanism and Applications. *Adv. Colloid Interface Sci.* **2022**, *308*, 102755. [[CrossRef](#)] [[PubMed](#)]
14. Huang, Y.; Long, B.; Tang, M.; Rui, Z.; Balogun, M.S.; Tong, Y.; Ji, H. Bifunctional catalytic material: An ultrastable and high-performance surface defect CeO<sub>2</sub> nanosheets for formaldehyde thermal oxidation and photocatalytic oxidation. *Appl. Catal. B Environ.* **2016**, *181*, 779–787. [[CrossRef](#)]
15. Koyaouli, T.-J. *Etude des Procédés Plasmas dans L'élimination des Polluants Organiques Persistants dans les Effluents Aqueux*. Ph.D. Thesis, University of Yaoundé I, Yaoundé, Cameroon, 2017.
16. Chen, H.; Mu, Y.; Shao, Y.; Chansai, S.; Xu, S.; Stere, C.E.; Xiang, H.; Zhang, R.; Jiao, Y.; Hardacre, C.; et al. Coupling non-thermal plasma with Ni catalysts supported on BETA zeolite for catalytic CO<sub>2</sub> methanation. *Catal. Sci. Technol.* **2019**, *9*, 4135–4145. [[CrossRef](#)]
17. Mohammed, S.S.; Shnain, Z.Y.; Abid, M.F. Use of TiO<sub>2</sub> in Photocatalysis for Air Purification and Wastewater Treatment: A Review. *Eng. Technol. J.* **2022**, *40*, 1131–1143. [[CrossRef](#)]
18. Serhane, Y.; Belkessa, N.; Bouzaza, A.; Wolbert, D.; Assadi, A.A. Continuous air purification by front flow photocatalytic reactor: Modelling of the influence of mass transfer step under simulated real conditions. *Chemosphere* **2022**, *295*, 133809. [[CrossRef](#)]
19. Belkessa, N.; Serhane, Y.; Bouzaza, A.; Khezami, L.; Assadi, A.A. Gaseous ethylbenzene removal by photocatalytic TiO<sub>2</sub> nanoparticles immobilized on glass fiber tissue under real conditions: Evaluation of reactive oxygen species contribution to the photocatalytic process. *Environ. Sci. Pollut. Res.* **2022**; ahead of print. [[CrossRef](#)] [[PubMed](#)]

20. Huang, Y.; Guo, Z.; Liu, H.; Zhang, S.; Wang, P.; Lu, J.; Tong, Y. Heterojunction Architecture of N-Doped WO<sub>3</sub> Nanobundles with Ce<sub>2</sub>S<sub>3</sub> Nanodots Hybridized on a Carbon Textile Enables a Highly Efficient Flexible Photocatalyst. *Adv. Funct. Mater.* **2019**, *29*, 1903490. [[CrossRef](#)]
21. Huang, Y.; Fan, W.; Long, B.; Li, H.; Zhao, F.; Liu, Z.; Tong, Y.; Ji, H. Visible light Bi<sub>2</sub>S<sub>3</sub>/Bi<sub>2</sub>O<sub>3</sub>/Bi<sub>2</sub>O<sub>2</sub>CO<sub>3</sub> photocatalyst for effective degradation of organic pollutions. *Appl. Catal. B Environ.* **2016**, *185*, 68–76. [[CrossRef](#)]
22. Chen, C.; Chen, F.; Zhang, L.; Pan, S.; Bian, C.; Zheng, X.; Meng, X.; Xiao, S.-H. Importance of platinum particle size for complete oxidation of toluene over Pt/ZSM-5 catalysts. *Chem. Commun.* **2015**, *51*, 5936–5938. [[CrossRef](#)]
23. Zhang, H.; Ma, D.; Qiu, R.; Tang, Y.; Du, C. Non-thermal plasma technology for organic contaminated soil remediation: A review. *Chem. Eng. J.* **2017**, *313*, 157–170. [[CrossRef](#)]
24. Mu, Y.; Xu, S.; Shao, Y.; Chen, H.; Hardacre, C.; Fan, X. Kinetic Study of Nonthermal Plasma Activated Catalytic CO<sub>2</sub> Hydrogenation over Ni Supported on Silica Catalyst. *Ind. Eng. Chem. Res.* **2020**, *59*, 9478–9487. [[CrossRef](#)]
25. Adelodun, A.A. Influence of Operation Conditions on the Performance of Non-thermal Plasma Technology for VOC Pollution Control. *J. Ind. Eng. Chem.* **2020**, *92*, 41–55. [[CrossRef](#)]
26. Qu, M.; Cheng, Z.; Sun, Z.; Chen, D.; Yu, J.; Chen, J. Non-thermal plasma coupled with catalysis for VOCs abatement: A review. *Process. Saf. Environ. Prot.* **2021**, *153*, 139–158. [[CrossRef](#)]
27. Li, S.; Dang, X.; Yu, X.; Abbas, G.; Zhang, Q.; Cao, L. The application of dielectric barrier discharge non-thermal plasma in VOCs abatement: A review. *Chem. Eng. J.* **2020**, *388*, 124275. [[CrossRef](#)]
28. Chen, M.; Jin, L.; Liu, Y.; Guo, X.; Chu, J. Decomposition of NO in automobile exhaust by plasma-photocatalysis synergy. *Environ. Sci. Pollut. Res.* **2014**, *21*, 1242–1247. [[CrossRef](#)] [[PubMed](#)]
29. Saoud, W.A.; Assadi, A.A.; Kane, A.; Jung, A.-V.; Le Cann, P.; Gerard, A.; Bazantay, F.; Bouzaza, A.; Wolbert, D. Integrated process for the removal of indoor VOCs from food industry manufacturing: Elimination of Butane-2,3-dione and Heptan-2-one by cold plasma-photocatalysis combination. *J. Photochem. Photobiol. Chem.* **2020**, *386*, 112071. [[CrossRef](#)]
30. Thevenet, F.; Sivachandiran, L.; Guaitella, O.; Barakat, C.; Rousseau, A. Plasmacatalyst coupling for volatile organic compound removal and indoor air treatment: A review. *J. Phys. Appl. Phys.* **2014**, *47*, 224011. [[CrossRef](#)]
31. Ye, H.; Liu, Y.; Chen, S.; Wang, H.; Liu, Z.; Wu, Z. Synergetic effect between non-thermal plasma and photocatalytic oxidation on the degradation of gas-phase toluene: Role of ozone. *Chin. J. Catal.* **2019**, *40*, 631–637. [[CrossRef](#)]
32. Li, K.; Lu, X.; Zhang, Y.; Liu, K.; Huang, Y.; Liu, H. Bi<sub>3</sub>TaO<sub>7</sub>/Ti<sub>3</sub>C<sub>2</sub> heterojunctions for enhanced photocatalytic removal of water-borne contaminants. *Environ. Res.* **2020**, *185*, 109409. [[CrossRef](#)]
33. Assadi, A.A.; Bouzaza, A.; Lemasle, M.; Wolbert, D. Removal of trimethylamine and isovaleric acid from gas streams in a continuous flow surface discharge plasma reactor. *Chem. Eng. Res. Des.* **2015**, *93*, 640–651. [[CrossRef](#)]
34. Shojaei, A.; Ghafourian, H.; Yadegarian, L.; Lari, K.; Sadatipour, M.T. Removal of volatile organic compounds (VOCs) from waste air stream using ozone assisted zinc oxide (ZnO) nanoparticles coated on zeolite. *J. Environ. Health Sci. Eng.* **2021**, *19*, 771–780. [[CrossRef](#)] [[PubMed](#)]
35. Abidi, M.; Hajjaji, A.; Bouzaza, A.; Lamaa, L.; Peruchon, L.; Brochier, C.; Rtimi, S.; Wolbert, D.; Bessais, B.; Assadi, A.A. Modeling of indoor air treatment using an innovative photocatalytic luminous textile: Reactor compactness and mass transfer enhancement. *Chem. Eng. J.* **2022**, *430*, 132636. [[CrossRef](#)]
36. Zeghioud, H.; Assadi, A.A.; Khellaf, N.; Djelal, H.; Amrane, A.; Rtimi, S. Reactive species monitoring and their contribution for removal of textile effluent with photocatalysis under UV and visible lights: Dynamics and mechanism. *J. Photochem. Photobiol. A Chem.* **2018**, *365*, 94–102. [[CrossRef](#)]
37. Assadi, A.A.; Bouzaza, A.; Wolbert, D. Photocatalytic oxidation of trimethylamine and isovaleraldehyde in an annular reactor: Influence of the mass transfer and the relative humidity. *J. Photochem. Photobiol. Chem.* **2012**, *236*, 61–69. [[CrossRef](#)]
38. García-Prieto, J.C.; González-Burciaga, L.A.; Proal-Nájera, J.B.; García-Roig, M. Kinetic Study and Modeling of the Degradation of Aqueous Ammonium/Ammonia Solutions by Heterogeneous Photocatalysis with TiO<sub>2</sub> in a UV-C Pilot Photoreactor. *Catalysts* **2022**, *12*, 352. [[CrossRef](#)]
39. Saoud, W.A.; Kane, A.; Le Cann, P.; Gerard, A.; Lamaa, L.; Peruchon, L.; Brochier, C.; Bouzaza, A.; Wolbert, D.; Assadi, A.A. Innovative photocatalytic reactor for the degradation of VOCs and microorganism under simulated indoor air conditions: Cu-Ag/TiO<sub>2</sub>-based optical fibers at a pilot scale. *Chem. Eng. J.* **2021**, *411*, 128622. [[CrossRef](#)]
40. Gharib-Abou Ghaida, S.; Assadi, A.A.; Costa, G.; Bouzaza, A.; Wolbert, D. Association of surface dielectric barrier discharge and photocatalysis in continuous reactor at pilot scale: Butyraldehyde oxidation, by-products identification and ozone valorization. *Chem. Eng. J.* **2016**, *292*, 276–283. [[CrossRef](#)]
41. Xu, P.; Ding, C.; Li, Z.; Yu, R.; Cui, H.; Gao, S. Photocatalytic degradation of air pollutant by modified nano titanium oxide (TiO<sub>2</sub>) in a fluidized bed photoreactor: Optimizing and kinetic modeling. *Chemosphere* **2023**, *319*, 137995. [[CrossRef](#)]
42. Rochetto, U.L.; Tomaz, E. Degradation of volatile organic compounds in the gas phase by heterogeneous photocatalysis with titanium dioxide/ultraviolet light. *J. Air Waste Manag. Assoc.* **2015**, *65*, 810–817. [[CrossRef](#)]
43. Cheng, Z.; Qu, M.; Chen, D.; Chen, J.; Yu, J.; Zhang, S.; Ye, J.; Hu, J.; Wang, J. Mechanisms of Active Substances in a Dielectric Barrier Discharge Reactor: Species Determination, Interaction Analysis, and Contribution to Chlorobenzene Removal. *Environ. Sci. Technol.* **2021**, *55*, 3956–3966. [[CrossRef](#)]
44. Sanito, R.C.; You, S.J.; Wang, Y.F. Degradation of contaminants in plasma technology: An overview. *J. Hazard. Mater.* **2022**, *424*, 127390. [[CrossRef](#)] [[PubMed](#)]



45. Petit, N.; Bouzaza, A.; Wolbert, D.; Petit, P.; Dussaud, J. Photocatalytic degradation of gaseous perchloroethylene in continuous flow reactors: Rate enhancement by chlorine radicals. *Catal. Today* **2007**, *124*, 266–272. [CrossRef]
46. Ebrahimi, H.; Shahna, F.G.; Bahrami, A.; Jaleh, B.; Abedi, K.A.D. Photocatalytic degradation of volatile chlorinated organic compounds with ozone addition. *Arch. Environ. Prot.* **2017**, *43*, 65–72. [CrossRef]
47. Ho, V.T.T.; Chau, D.H.; Bui, K.Q.; Nguyen, N.T.T.; Tran, T.K.N.; Bach, L.G.; Truong, S.N. A High-Performing Nanostructured Ir Doped-TiO<sub>2</sub> for Efficient Photocatalytic Degradation of Gaseous Toluene. *Inorganics* **2022**, *10*, 29. [CrossRef]
48. Ghorbani Shahna, F.; Bahrami, A.; Alimohammadi, I.; Yarahmadi, R.; Jaleh, B.; Gandomi, M.; Ebrahimi, H.; Ad-Din Abedi, K. Chlorobenzene degeradation by non-thermal plasma combined with EG-TiO<sub>2</sub>/ZnO as a photocatalyst: Effect of photocatalyst on CO<sub>2</sub> selectivity and byproducts reduction. *J. Hazard. Mater.* **2017**, *324*, 544–553. [CrossRef]
49. Gao, L.; Jiang, Y.; Ye, K.; Deng, B. A Study on the Effects of Operating Parameters on the Degradation of Oxalic Acid in a Photocatalytic Reactor using Computational Fluid Dynamics. *Pollution* **2023**, *9*, 579–590.
50. Kulawik, P.; Rathod, N.B.; Ozogul, Y.; Ozogul, F.; Zhang, W. Recent developments in the use of cold plasma, high hydrostatic pressure, and pulsed electric fields on microorganisms and viruses in seafood. *Crit. Rev. Food Sci. Nutr.* **2022**; ahead of print. [CrossRef]
51. Assadi, A.A.; Bouzaza, A.; Vallet, C.; Wolbert, D. Use of DBD plasma, photocatalysis, and combined DBD plasma/photocatalysis in a continuous annular reactor for isovaleraldehyde elimination—Synergetic effect and byproducts identification. *Chem. Eng. J.* **2014**, *254*, 124–132. [CrossRef]
52. Dahiru, U.H.; Saleem, F.; Zhang, K.; Harvey, A. Plasma-assisted removal of methanol in N<sub>2</sub>, dry and humidified air using a dielectric barrier discharge (DBD) reactor. *RSC Adv.* **2022**, *12*, 10997–11007. [CrossRef]
53. Hatzisymeon, M.; Tataraki, D.; Tsakiroglou, C.; Rassias, G.; Aggelopoulos, C.A. Highly energy-efficient degradation of antibiotics in soil: Extensive cold plasma discharges generation in soil pores driven by high voltage nanopulses. *Sci. Total Environ.* **2021**, *786*, 147420. [CrossRef]
54. Wei, B.; Chen, Y.; Ye, M.; Shao, Z.; He, Y.; Shi, Y. Enhanced Degradation of Gaseous Xylene Using Surface Acidized TiO<sub>2</sub> Catalyst with Non-thermal Plasmas. *Plasma Chem. Plasma Process.* **2015**, *35*, 173–186. [CrossRef]
55. Ansari, M.; Sharifian, M.; Ehrampoush, M.H.; Mahvi, A.H.; Salmani, M.H.; Fallahzadeh, H. Dielectric barrier discharge plasma with photocatalysts as a hybrid emerging technology for degradation of synthetic organic compounds in aqueous environments: A critical review. *Chemosphere* **2021**, *263*, 128065. [CrossRef] [PubMed]
56. Qi, L.-Q.; Yu, Z.; Chen, Q.-H.; Li, J.-X.; Xue, H.-B. Toluene degradation using plasma-catalytic hybrid system over Mn-TiO<sub>2</sub> and Fe-TiO<sub>2</sub>. *Sci. Pollut. Res.* **2022**, 23494–23509. Available online: <https://link.springer.com/10.1007/s11356-022-23834-8> (accessed on 5 February 2023). [CrossRef] [PubMed]
57. Khezami, L.; Nguyen-Tri, P.; Saoud, W.A.; Bouzaza, A.; El Jerry, A.; Nguyen, D.D.; Gupta, V.K.; Assadi, A.A. Recent progress in air treatment with combined photocatalytic/plasma processes: A review. *J. Environ. Manag.* **2021**, *299*, 113588. [CrossRef] [PubMed]
58. Chen, J.; Liu, J.; Liu, X.; Gao, W.; Zhang, J.; Zhong, F. Degradation of toluene in surface dielectric barrier discharge (SDBD) reactor with mesh electrode: Synergistic effect of UV and TiO<sub>2</sub> deposited on electrode. *Chemosphere* **2022**, *288*, 132664. [CrossRef] [PubMed]
59. Gopi, T.; Swetha, G.; Shekar, S.C.; Krishna, R.; Ramakrishna, C.; Saini, B.; Rao, P. Ozone catalytic oxidation of toluene over 13X zeolite supported metal oxides and the effect of moisture on the catalytic process. *Arab. J. Chem.* **2019**, *12*, 4502–4513. [CrossRef]
60. Attri, P.; Koga, K.; Okumura, T.; Chawarambwa, F.L.; Putri, T.E.; Tsukada, Y.; Kamataki, K.; Itagaki, N. Treatment of organic wastewater by a combination of non-thermal plasma and catalyst: A review. *Rev. Mod. Plasma Phys.* **2022**, *6*, 17. [CrossRef]
61. Poormohammadi, A.; Bashirian, S.; Rahmani, A.R.; Azarian, G.; Mehri, F. Are photocatalytic processes effective for removal of airborne viruses from indoor air? A narrative review. *Environ. Sci. Pollut. Res.* **2021**, *28*, 43007–43020. [CrossRef]
62. Bhargavi, K.V.S.S.; Ray, D.; Chawdhury, P.; Rajanikanth, B.S.; Thatikonda, S.; Challapalli, S. Catalytic non-thermal plasma reactor for oxidative degradation of toluene present in low concentration. *Catal. Today*, **2023**; in press.
63. Piferi, C.; Daghetta, M.; Schiavon, M.; Roman, H.E.; Riccardi, C. Pentane Depletion by a Surface DBD and Catalysis Processing. *Appl. Sci.* **2022**, *12*, 4253. [CrossRef]
64. Palaun, J.; Assadin, A.A.; Penya-rojan, J.M.; Bouzazan, A.; Wolbert, D.; Martínez-Sorian, V. Isovaleraldehyde degradation using UV photocatalytic and dielectric barrier discharge reactors, and their combinations. *J. Photochem. Photobiol. A Chem.* **2015**, *299*, 110–117.
65. Huang, H.; Lu, H.; Zhan, Y.; Liu, G.; Feng, Q.; Huang, H.; Wu, M.; Ye, X. VUV photo-oxidation of gaseous benzene combined with ozone-assisted catalytic oxidation: Effect on transition metal catalyst. *Appl. Surf. Sci.* **2017**, *391*, 662–667. [CrossRef]
66. Machniewski, P.; Biń, A.; Kłosek, K. Effectiveness of toluene mineralization by gas-phase oxidation over Co(II)/SiO<sub>2</sub> catalyst with ozone. *Environ. Technol.* **2021**, *42*, 3987–3994. [CrossRef] [PubMed]
67. Assadi, A.A.; Loganathan, S.; Tri, P.N.; Ghaida, S.G.-A.; Bouzaza, A.; Tuan, A.N.; Wolbert, D. Pilot scale degradation of mono and multi volatile organic compounds by surface discharge plasma/TiO<sub>2</sub> reactor: Investigation of competition and synergism. *J. Hazard. Mater.* **2018**, *357*, 305–313. [CrossRef]

**Disclaimer/Publisher’s Note:** The statements, opinions and data contained in all publications are solely those of the individual author(s) and contributor(s) and not of MDPI and/or the editor(s). MDPI and/or the editor(s) disclaim responsibility for any injury to people or property resulting from any ideas, methods, instructions or products referred to in the content.